A Multi-scale model for CO_2 capture: A Nickel-based oxygen carrier in Chemical-looping Combustion

Huabei You, Yue Yuan, Jingde Li, Luis Ricardez Sandoval

Department of Chemical Engineering, University of Waterloo,
Waterloo, Canada (e-mail: laricard@uwaterloo.ca)

Abstract: In this work, we present a multi-scale modelling framework for the Ni-based oxygen carrier (OC) particle that can explicitly account for the complex reaction mechanism taking place on the contacting surface between gas and solid reactants in Chemical Looping Combustion (CLC). This multi-scale framework consists of a gas diffusion model and a surface reaction model. Continuum equations are used to describe the gas diffusion inside OC particles, whereas Mean-field approximation method is adopted to simulate the micro-scale events, such as molecule adsorption and elementary reaction, occurring on the contacting surface. A pure CO stream is employed as the fuel gas whereas the NiO is used as the metal oxide because it is one of the mostly used material in laboratory and pilot-scale plants. Rate constants for the micro-scale events considered in the present work were obtained from a systematic Density Functional Theory (DFT) analysis, which provides a reasonable elementary reaction kinetics and lays a solid foundation for multi-scale calculations. A sensitivity analysis on the size of intra-particle pore and the adsoprtion rate constant was conducted to assess the mass transport effects on the porous particle. The proposed multi-scale model shows reasonable tendencies and responses to changes in key modelling parameters.

Keywords: Multi-scale model, Heterogeneous modelling, CO_2 capture, Chemical-looping combustion, Oxygen carrier.

1. INTRODUCTION

Chemical-looping combustion (CLC) is one of the most promising greenhouse gas emission control technologies. The concept of chemical looping involves the use of a metal oxide as the oxygen carrier (OC) which continuously circulates between a fuel-reactor, where the OC provides oxygen to burn the fuel, and an air-reactor, where the OC is oxidized with air. Compared to the traditional fuel combustion process, CLC does not require extra separation units to obtain a pure CO_2 stream, thus minimizing the energy penalty associated with CO_2 capture process.

In order to design, optimize, and eventually scale-up the CLC process, a variety of the fuel- and air-reactors models have been developed. The three main parameters for the design of reactors in CLC process are: (1) the total load of bed material; (2) the circulation rate of the bed material; and (3) the gas leakage between two reactors (Lyngfelt et al., 2001). The first two parameters directly depend on the performance of the selected oxygen carrier.

The ideal oxygen carrier should have the following properties: high reactivity; resistance against carbon deposition; high mechanical strength; and sufficient stability in successive cycle reactions. Particles made of pure metal oxide do not have enough mechelical strength and also tend to form agglomerations. However, this problem can be avoided by combining the metal oxide with another inert support material. On the other hand, the main issue that most of the common OC particles have is that reaction and conversion rates often decrease after a few (or several) CLC cycles. Thus, having access to an OC model that can evaluate the impact of the reaction kinetics on the overall performance of the OC particle will greatly help the modelling of CLC process which can demonstrate the technical viability of this emerging technology for CO_2 capture and clean power generation.

The most common OC models available in the literature are the Shrinking Unreacted Core Model(Ryu et al., 2001), the Changing Grain Size Model (García-Labiano et al., 2005), and the Nucleation and Nuclei Growth Model (Hossain and de Lasa, 2010). The Shrinking Unreacted Core Model depicts the oxygen carrier particle as a spherical grain made of the solid reactant (metal oxide). Reactions initially take place at the outer surface of the unreacted solid which keeps moving inward as the reaction proceeds. The Changing Grain Size Model assumes that the oxygen carrier particle is a mixture of metal oxide grains and inert support grains; the fuel gas diffuses through the interstices between grains, i.e. the particle's pore, and reacts with the metal oxide grains representing by the Shrinking Unreacted Core Model. Furthermore, the Nucleation and Nuclei Growth Model assumes that all reactions inside the oxygen carrier particle are initiated by the formation of nuclei in the solid phase and then continue with subsequent growth of the formed nuclei. The reaction rate is calculated using a function that contains parameters estimated by fitting the model with experimental data.

The OC particle models described above have been used to simulate the temperature and conversion profiles inside some common oxygen carriers during the CLC process. The simulation results were found to be in reasonable agreement with experimental data. These models have assumed that the concentration of gas reactant only varies in one direction that is normal to the particle surface. These models have also considered that the chemical reactions can be simplified as first order reactions with respect to the concentration of gas species. In a real setting, concentration profiles in both axial and radial directions exist when the gas (i.e. the fuel) diffuses through the particle's pore. Moreover, reactions are actually taking place on the solid surface, and the mechanism is generally more complex than first order reactions. Therefore, these models are not able to describe the impact of radial concentration gradients across the pore and the complexity of reaction kinetics which, as suggested by experimental results, plays an important role and should be taken into account when developing oxygen carrier particle models (Dueso et al., 2012).

The difficulty in modelling the impact of reaction kinetics lies in the discrepancies between the evolution of the chemical reactions on the particle's surface and the continuum mechanics that describes the transport of molecules in the gas phase. Specifically, the gas diffusion in the pore occurs at the micrometer length scale whereas the surface events are usually taking place in atomic dimensions. In addition, the corresponding time scale for the chemical reactions is also orders of magnitude smaller than that for gas diffusion. As a result, simulating gas diffusion and surface reaction simultaneously throughout the entire spacial domain is computationally intensive. To tackle this problem, Vlachos (1997) assessed the numerical feasibility of multi-scale integration hybrid (MIH) algorithms that links a unimolecular surface reaction model to a macroscopic species transportation model by decomposing the system into two partially overlapping subdomains. To the authors' knowledge, multi-scale models that predict events taking place inside the OC in CLC has not been proposed in the literature.

The present work presents a multi-scale framework for oxygen carrier particle in Chemical-looping combustion. Nickel oxide is selected to be the solid reactant in oxygen carrier because it is a common oxygen carrier used for laboratory and pilot-scale demonstration plants and exhibits high reactivity and stability (Mattisson et al., 2006). For simplicity, the fuel gas in this work only contains carbon oxide. The proposed multi-scale model for Ni-based oxygen carrier used in CLC process is presented in the next section.

2. MODEL DEVELOPMENT

The overall configuration of the multi-scale model is illustrated in Figure 1. The oxygen carrier is considered to be a spherical particle with numerous cylindrical pores. Fuel gas enters the particle through the inlet of the pore and diffuses in both axial (z) and radial (r) directions.

When a gas molecule reaches the inner wall of the pore (i.e., boundary in the r-direction), it will either stay in the gas phase or get adsorbed onto the wall surface. The
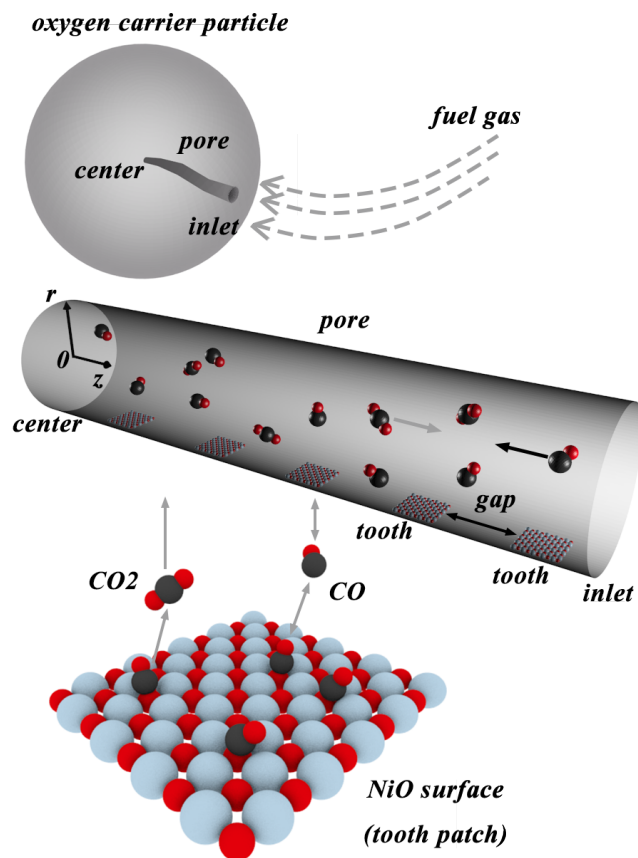

Fig. 1. Schematic of the present multi-scale model.

adsorbed molecules will react with the solid reactant on the surface and release the product into the gas phase. The gas concentration profile in radial and axial directions within the pore is calculated using mass conservation equations (i.e. gas phase model). The surface reactions are simulated by a surface model using the Mean-field approximation method (Kevrekidis et al., 1984). The gas phase model and the surface model are coupled through a mass flux boundary condition located at the top of the surface, i.e. above the pore's inner walls.

The following assumptions are adopted in the model:

(1) Structure of the OC particles does not change during the reaction.
(2) OC particles are considered isothermal.
(3) Mass transport through the particle only occurs by diffusion.
(4) OC particles are surrounded by fuel gas and the gas concentration remain constant during the CLC process.

2.1 Gas Diffusion Model

The two dimensional unsteady-state mass transport of molecules in the gas phase is described by the continuum equation:

$$\frac{\partial C_i}{\partial t} = \mathcal{D}_{e,i} \frac{1}{r} \frac{\partial}{\partial r}\left(r \frac{\partial C_i}{\partial r}\right) + \mathcal{D}_{e,i} \frac{\partial^2 C_i}{\partial z^2}. \tag{1}$$

with the following initial and boundary conditions:

$$C_i(t,z,r)\big|_{t=0} = 0 \qquad (2)$$

$$\frac{\partial C_i(t,z,r)}{\partial z}\bigg|_{z=0} = 0 \qquad (3)$$

$$\frac{\partial C_i(t,z,r)}{\partial r}\bigg|_{r=0} = 0 \qquad (4)$$

$$-\mathcal{D}_{e,i}\frac{\partial C_i(t,z,r)}{\partial z}\bigg|_{z=L} = k_{g,i}\left(C_i(t,z,r)\big|_{z=L} - C_i^{bulk}\right) \qquad (5)$$

$$-\mathcal{D}_{e,i}\frac{\partial C_i(t,z,r)}{\partial r}\bigg|_{r=R} = -k_{a,i}C_i(t,z,r)\big|_{r=R}\theta_{empty}(t)\big|_z$$
$$+ \frac{C_T}{N_A}k_{r,i}\theta_i(t) \qquad (6)$$

where C_i is concentration of gas i in the pore; r and z are the radial and axial domains representing; R and L are the pore radius and pore length, respectively; $\mathcal{D}_{e,i}$ is the effective diffusivity of gas i in the pore; $k_{g,i}$ is the external mass transfer coefficient of gas species i; C_i^{bulk} is the bulk concentration of gas i; θ_{empty} is the surface coverage of empty sites on the surface; θ_i is the surface coverage of surface species i; $k_{a,i}$ is the adsorption rate constant of surface species i; $k_{r,i}$ is the reaction rate constant of surface species i; C_T is the density of surface sites; N_A is the Avogadro's number.

The effective diffusivity of gas i was calculated as a function of gas diffusivity and particle porosity:

$$\mathcal{D}_{e,i} = \mathcal{D}_{g,i}\varepsilon^2 \qquad (7)$$

where ε is the pore porosity.

When gas diffuses through the pore, molecular diffusion and Knudsen diffusion are both present. Therefore, gas diffusivity was calculated as follows:

$$\mathcal{D}_{g,i} = \left(\frac{1}{\mathcal{D}_{m,i}} + \frac{1}{\mathcal{D}_{K,i}}\right)^{-1} \qquad (8)$$

where the molecular diffusivity $\mathcal{D}_{m,i}$ and the Knudsen diffusivity $\mathcal{D}_{K,i}$ are calculated using the following correlations (Fuller et al., 1966):

$$\mathcal{D}_{m,i} = \frac{1.0\times 10^{-7}T^{1.75}\left(M_i^{-1} + M_S^{-1}\right)^{0.5}}{P\left[(\sum_i \nu_i)^{1/3} + (\sum_S \nu_i)^{1/3}\right]^2} \qquad (9)$$

$$\mathcal{D}_{K,i} = \frac{2}{3}r\sqrt{\frac{8RT}{\pi M_i}} \qquad (10)$$

where T is the temperature in Kelvin; M_i is the molecular weight of gas i; M_S is the molecular weight of the solvent S; P is the pressure in atm; ν_i is the diffusion parameters of the diffusing species.

The external mass transfer coefficient k_g was calculated using Sherwood number:

$$k_{g,i} = \frac{\mathcal{D}_{m,i}Sh}{d_{par}} \qquad (11)$$

where Sh is the Sherwood number; d_{par} is the particle diameter.

The surface coverage fractions of empty sites and surface species i at each point in time across the axial domain is determined from the surface model (see *Section 2.2*).

Kinetics parameters are obtained from density functional theory (DFT) simulations (see *Kinetic Parameters* section).

Table 1 shows the parameters used in this study. The surface site density C_T was published by Okazawa et al. (2007) whereas the operating conditions were taken from Adánez et al. (2012). These conditions are representative of pilot-scale CLC plants.

Table 1. Model Parameters

Parameters (Unit)	Values
Temperature, T (K)	1173
Pressure, P (atm)	1
Particle radius (Pore length), L (m)	1.0×10^{-4}
Pore radius, R (m)	1.0×10^{-8}
Porosity, ε	0.4
Effective Diffusivity of CO, $\mathcal{D}_{e,CO}$ (m$^2\cdot$s^{-1})	9.775×10^{-7}
Effective Diffusivity of CO$_2$, $\mathcal{D}_{e,CO_2}$ (m$^2\cdot$s^{-1})	7.796×10^{-7}
Density of sites, C_T (sites$\cdot$m^{-2})	1.33×10^{19}
Bulk gas concentration, C_{CO}^{bulk} (mol$\cdot$m^{-3})	10.0
Bulk gas concentration, $C_{CO_2}^{bulk}$ (mol$\cdot$m^{-3})	0.0
Sherwood number, Sh	7

2.2 Surface Model

As shown in Figure 1, The pore surface is considered to be a finite square lattice. Each lattice site can be occupied by at most one molecule through adsorption. According to the results from DFT simulations, CO molecules tend to attach to the oxygen atoms on the exposed NiO surface and form a $NiO - CO$ micro-structure. After formation of $NiO - CO$, CO captures the oxygen atom in NiO and becomes CO_2. The desorption of CO_2 is considered to be much faster than the proceding reactions; thus, this step is not considered explicitly in the present model. Therefore, the reaction mechanisms used in the present work involves two steps: A CO molecule in gas phase adsorbs onto an empty site on the surface (i.e. an available oxygen atom); and the adsorbed CO reacts with NiO and produces CO_2:

$$CO(g) + NiO* \xrightarrow{k_a} NiO - CO* \qquad (12)$$

$$NiO - CO* \xrightarrow{k_r} Ni* + CO_2(g) \qquad (13)$$
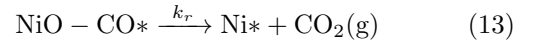
where $*$ denotes an empty site on the surface.

The present mechanism assumes that the oxygen on the surface is in excess during the time period in the simulation and the CO_2 molecule leaves the surface instantly after it was formed. Hence, CO molecules always have access to oxygen atoms and no CO_2 molecule will stay on the surface (the surface coverage of CO_2 is zero).

Mean Field Approximation Mean-field approximation assumes that the adsorbed molecules are distributed homogeneously on the surface. The effect of the surface configuration on a single adsorbate is approximated by the average occupancy of lattice sites by any of the adsorbed molecules. The rate of change of the surface concentration of species i (C_i^{surf}) can be described as the rate of adsorption minus the rate of consumption:

$$\frac{dC_i^{surf}(t)}{dt} = k_{a,i}C_i\big|_{r=R}\left(1 - \sum_{j=1}^{n}\theta_j(t)\right)$$
$$- \sum_k k_{r,i}C_i^{surf}(t) \tag{14}$$

Equation 14 can also be expressed in terms of the surface coverage fraction as follows:

$$\frac{d\theta_i(t)}{dt} = \frac{N_A}{C_T}k_{a,i}C_i\big|_{r=R}\left(1 - \sum_{j=1}^{n}\theta_j(t)\right)$$
$$- \sum_i k_{r,i}\theta_i(t) \tag{15}$$

where $C_i\big|_{r=R}$ is concentration of gas i above the surface and is estimated from the gas phase model; n is the number of surface species ($n = 1$ in this framework).

The sum of the coverage fraction of all surface species and empty sites will always be equal to one; therefore, the following equation is also valid in the Mean-field approximation:

$$1 = \theta_{empty}(t) + \sum_{i=1}^{n}\theta_i(t) \tag{16}$$

For the proposed reaction mechanisms, the following equations are considered in the present surface model:

$$\frac{d\theta_{CO}(t)}{dt} = \frac{N_A}{C_T}k_aC_{CO}\big|_{r=R}\theta_{empty} - k_r\theta_{CO}(t) \tag{17}$$

$$1 = \theta_{empty}(t) + \theta_{CO}(t) \tag{18}$$

Kinetic Parameters. Density functional theory (DFT) is carried out to calculate the kinetic parameters used in this work using Vienna Ab Initio Simulation Package (VASP). The projector-augmented wave (PAW) method (Blöchl, 1994) with the generalized gradient approximation of Perdew-Burke-Ernzerhof (Perdew et al., 1996) is chosen to describe the system. To simulate the reactions, a 6-layer nickel oxide slab model is constructed while the 2 bottom layers are fixed. Through structural relaxation and nudged-elastic-band method (Henkelman et al., 2000), we have established the 2-step carbon monoxide oxidation mechanism discussed in the previous section.

2.3 Model Coupling

In the present work, the gap-tooth method (Gear et al., 2003) is adopted to compute the concentration gradients across the pore's axial domain. As shown in Fig. 1, the tooth represents the surface model placed at equally-spaced discrete points in the axial domain of the multi-scale model whereas the gap is the length between two subsequent teeth (i.e. surface models).

The implicit backward Euler discretization has been employed to solve for the gas diffusion model. The number of teeth (surface models) considered in this system matches with the discretized nodes in the z-direction of the gas phase model. At time $t = t'$, the surface coverage of molecule i on a tooth patch located at the specific node (z', R) is determined using the surface model (Eq. 17 to 18). Note that the concentration of gas species i at that same

node point $C_i(t', z', R)$ represents the input to the surface model. The calculated coverage $\theta_i\big|_{t=t'}$ at node (z', R) is needed to evaluate the gas phase boundary condition (Eq. 6) and provides the mass flux at node (z', R). The later is required to solve for the gas diffusion model (Eq. 1) for the next time interval. The number of teeth points required to solve the model is problem-specific. The present work used ten teeth to obtain a trade-off between numerical accuracy and computational cost.

This coupling scheme is based on the interaction between the gas diffusion model and the surface model - the concentration of gas species i above the surface affects the surface configuration through the adsorption term in Eq. 15, which in turn determines the adsorption rates that enter into the boundary condition of the gas diffusion model (Eq. 6).

3. RESULTS AND ANALYSIS

The multi-scale model presented in the previous section was implemented in Python 3.6; Each simulation requires approximately 574 CPU seconds (3.4GHz Intel i7-3770 processor). Because of the scarcity of similar OC particle models and comparable experimental data, model validation cannot be performed at this time. Therefore, we carried out a sensitivity analysis on the key modelling parameters to evaluate their effects on the system's behavior.

Table 2 shows the kinetic parameters obtained from DFT simulations. To obtain the reaction rate constants for this process, we screened multiple configurations and found the most stable structures from DFT analysis for reactants and products in the surface reaction system (not discussed here for brevity). Transition states of this 2-step-reaction are searched as saddle points, which are confirmed by frequency calculations. The rate constants are calculated using the same temperature used in the gas diffusion model ($1173K$); The parameters presented in Table 1 and 2 are considered to be the reference condition.

The rate of reactions taking place inside the OC particle depends on several factors such as the physical properties of the particles (particle size, porosity, composition, etc.) and chemical kinetics of the reactions. The effects of the pore size and the adsorption rate constant on the CO conversion rate and the surface reaction rates were assessed using the concentration profile at the center point in the outlet ($z = 0$, $r = 0$) (see Fig. 1). As shown in Fig. 2 and 4 (red line), the CO concentration at that center point reached steady state within one second, whereas 30 seconds are needed for the CO_2 concentration to reach steady state (see the red line in Fig. 3 and 5). These results suggest that the rate of gas diffusion is not controlling the rates of surface reactions that consume CO and produce CO_2.

Table 2. Kinetic Parameters

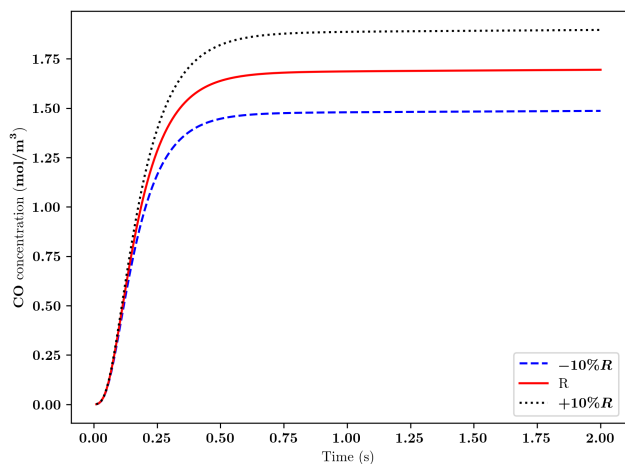| Parameters (Unit)	Values
CO adsorption rate constant, k_a (m · s^{-1})	2.90×10^{-6}
CO_2 formation rate constant, k_r (s^{-1})	3.13

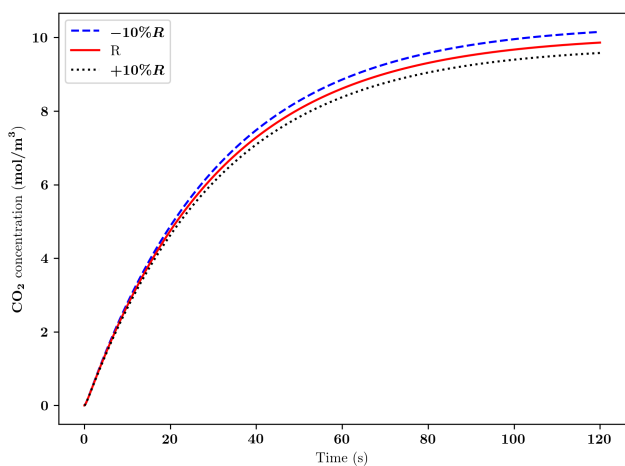Fig. 2. Effect of the varying pore radius on the evolution of CO concentration at the center of the particle.

Fig. 4. Effect of k_a on the evolution of CO concentration at the center of the particle.

Fig. 3. Effect of the varying pore radius on the evolution of CO_2 concentration at the center of the particle.

Fig. 5. Effect of k_a on the evolution of CO_2 concentration at the center of the particle.

3.1 Effect of the pore size

Figure 2 shows the impact of pore radius on the consumption rate of CO. The evolution of CO concentration at the center of the end of the pore (i.e. the center of the OC particle) was simulated using a +/- 10% change in the pore radius on each simulation; steady state was achieved within one second in all three cases (see Fig. 2). The result shows that CO concentration at steady state within a larger pore is higher than that obtained for a smaller pore. This behavior is expected because increasing pore size also promotes mass transport, thus enhancing the diffusion process. On the other hand, concentration of CO_2 reached steady state after 120 seconds in all three simulations using a +/- 10% change in the pore radius. Compared to Fig. 2, increasing the CO concentration did not lead to an increase in the steady state CO_2 concentration. However, note that the concentration at the center point will also be affected by the radial gas diffusion. That is, a larger pore radius leads to a longer distance between the inner wall of the pore (i.e. pore surface) to that center point. Hence, a longer period of time is required for the product generated on the pore surface to reach the center of the pore. Therefore, it is reasonable to consider that the gas diffusion taking place
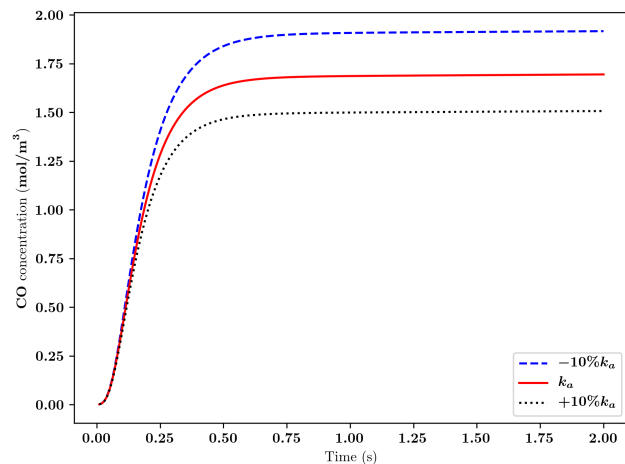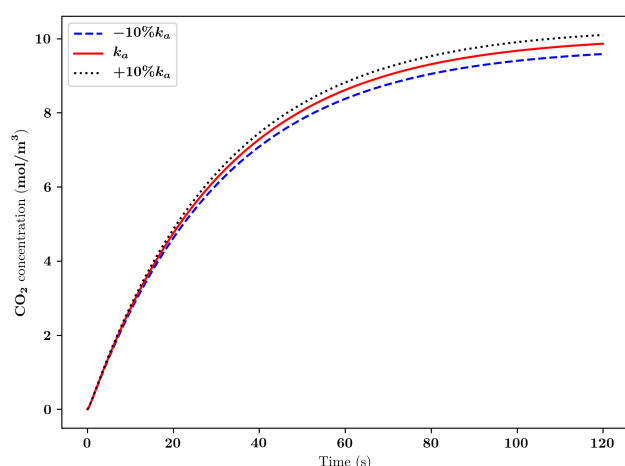
in the radial direction causes the CO_2 concentration at the center of a larger pore to be lower than that of a smaller pore.

3.2 Effect of the adsorption rate constant

The limiting step for reactions in the present model is CO adsorption as the adsorption rate constant k_a is 10^6 magnitude smaller than the CO_2 formation rate constant k_r. To analyze the effect of this variable on the extent of reaction inside the particle, several simulations were carried out using different adsorption rate constants ranging from -10% to +10%.

The results show that the concentration of CO reached steady state within one second. The steady state concentration of the reactant gas CO increased by 13% when the adsorption rate constant decreased by 10% (see Fig. 4). Correspondingly, when k_a decreased, the concentration of gas product CO_2 at steady state also decreased, as a smaller k_a means CO molecules in the gas phase are less likely to adsorb onto the surface; and the decrease in available adsorbed CO molecules will slow down the CO_2 formation reaction.
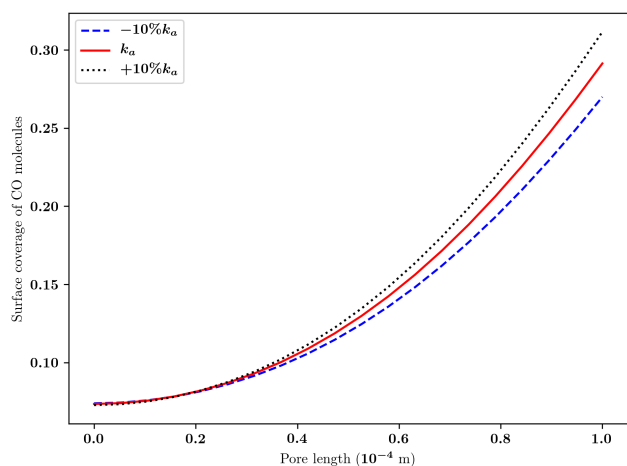
Fig. 6. Effect of the adsorption rate constant k_a on the CO surface coverage in the axial direction.

Furthermore, the surface coverage of CO at equally-spaced teeth points in the axial direction was evaluated after the concentration of CO and CO_2 both reached steady state (see Fig. 6). As expected, the surface coverage of CO at the inlet of the pore (Pore length $= 1.0 \times 10^{-4}$) was higher than that at the end of the pore due to the higher inlet concentration. Moreover, increasing the adsorption rate constant increased the surface coverage at each tooth point, which agrees with the decrease in the steady state concentration of CO (Fig. 4) as more CO molecules will diffuse from the gas phase and adsorb onto the pore surface.

Note that the CO surface coverage did not reach the steady state after 120 seconds, whereas the CO concentration reached the steady state within 1 second. That is, the increasing amount of available CO molecules on the surface did not increase its consumption rate substantially. This indicates that, although the adsorption rate constant is significantly smaller than the reaction rate constant, the latter may be the rate controlling parameter in the initial stages of this process.

4. CONCLUSION

A multi-scale particle model framework consisting of a gas diffusion model and a surface reaction model has been developed for oxygen carrier particles used in a typical CLC system. Chemical reaction kinetics is explicitly considered in the surface model using reaction rate constants obtained from DFT analysis. NiO was selected to be the solid reactant that provides oxygen, and a pure CO stream was assumed to be the gas reactant (fuel gas). This model was then used to predict the influence of pore size and adsorption rate constant on the steady state concentration profile of the gas species inside the particle. Currently, due to the lack of similar OC particle models or experimental data for the simulated NiO system, model validation will be considered in the future work. The sensitivity analysis showed reasonable tendencies and responses to changes in key modelling parameters, which indicates the feasibility of this model.

The present multi-scale particle model framework will be further developed in the following aspects: Syngas (CO and H_2) will be used to replace the pure CO stream considered in this work; also more reaction details will be considered; Kinetic Monte Carlo (KMC) method will be employed to simulate the many-body interactions taking place in the pore's surface.

REFERENCES

Adánez, J., Abad, A., García-Labiano, F., Gayán, P., and de Diego, L.F. (2012). Progress in chemical-looping combustion and reforming technologies. *Progress in Energy and Combustion Science*, 38(2), 215–282.

Blöchl, P.E. (1994). Projector augmented-wave method. *Physical Review B*, 50(24), 17953–17979.

Dueso, C., Ortiz, M., Abad, A., García-Labiano, F., de Diego, L.F., Gayán, P., and Adánez, J. (2012). Reduction and oxidation kinetics of nickel-based oxygen-carriers for chemical-looping combustion and chemical-looping reforming. *Chemical Engineering Journal*, 188, 142–154.

Fuller, E.N., Schettler, P.D., and Giddings, J.C. (1966). New Method for Prediction of Binary Gas-phase Diffusion Coefficients. *Industrial & Engineering Chemistry*, 58(5), 18–27.

García-Labiano, F., de Diego, L.F., Adánez, J., Abad, A., and Gayán, P. (2005). Temperature variations in the oxygen carrier particles during their reduction and oxidation in a chemical-looping combustion system. *Chemical Engineering Science*, 60(3), 851–862.

Gear, C., Li, J., and Kevrekidis, I.G. (2003). The gap-tooth method in particle simulations. *Physics Letters A*, 316(3), 190–195.

Henkelman, G., Uberuaga, B.P., and Jónsson, H. (2000). A climbing image nudged elastic band method for finding saddle points and minimum energy paths. *The Journal of Chemical Physics*, 113(22), 9901–9904.

Hossain, M.M. and de Lasa, H.I. (2010). Reduction and oxidation kinetics of Co-Ni/Al$_2$O$_3$ oxygen carrier involved in a chemical-looping combustion cycles. *Chemical Engineering Science*, 65(1), 98–106.

Kevrekidis, I., Schmidt, L., and Aris, R. (1984). Rate multiplicity and oscillations in single species surface reactions. *Surface Science*, 137(1), 151 – 166.

Lyngfelt, A., Leckner, B., and Mattisson, T. (2001). A fluidized-bed combustion process with inherent CO_2 separation; application of chemical-looping combustion. *Chemical Engineering Science*, 56(10), 3101 – 3113.

Mattisson, T., Johansson, M., and Lyngfelt, A. (2006). The use of NiO as an oxygen carrier in chemical-looping combustion. *Fuel*, 85(5-6), 736–747.

Okazawa, T., Nishizawa, T., Nishimura, T., and Kido, Y. (2007). Oxidation kinetics for Ni(111) and the structure of the oxide layers. *Phys. Rev. B*, 75, 033413.

Perdew, J.P., Burke, K., and Ernzerhof, M. (1996). Generalized Gradient Approximation Made Simple. *Physical Review Letters*, 77(18), 3865–3868.

Ryu, H.J., Bae, D.H., Han, K.H., Lee, S.Y., Jin, G.T., and Choi, J.H. (2001). Oxidation and reduction characteristics of oxygen carrier particles and reaction kinetics by unreacted core model. *Korean Journal of Chemical Engineering*, 18(6), 831–837.

Vlachos, D.G. (1997). Multiscale integration hybrid algorithms for homogeneous–heterogeneous reactors. *AIChE Journal*, 43(11), 3031–3041.